Ternary Na-P-H superconductor under high pressure

Ternary Na-P-H superconductor under high pressure

Weiguo Sun,[1,2] Bole Chen,[3] Xiaofeng Li,[1] Feng Peng,[1,*] Andreas Hermann,[4] and Cheng Lu[2,†]

[1] *College of Physics and Electronic Information, Luoyang Normal University, Luoyang 471022, China*
[2] *School of Mathematics and Physics, China University of Geosciences (Wuhan), Wuhan 430074, China*
[3] *School of Science, Chongqing University of Posts and Telecommunications, Chongqing 400065, China*
[4] *Centre for Science at Extreme Conditions and SUPA, School of Physics and Astronomy, University of Edinburgh, Edinburgh, EH9 3FD, United Kingdom*

(Dated: May 30, 2023)

Most of the H-rich superconductors are discovered so far to be clathrate structures. Several clathrate hydrides, including H_3S, LaH_{10} and CaH_6, are predicted as excellent superconductors through structural searches and later confirmed through experimental synthesis. Here, we conduct extensively crystal structure searches and first-principles calculations for ternary Na-P-H hydrides under high pressure. Two stoichiometries of $NaPH_6$ and $NaPH_8$ in ternary Na-P-H hydrides are found to be stable under 200 GPa. The $P\bar{6}m2$ phase of $NaPH_6$ hydride is identified as the novel ternary layered H-rich superconductor, exhibiting a high critical temperature (T_c) of 112.2 K under 200 GPa. Our calculations indicate that the high T_c of $NaPH_6$ hydride under high pressure is attributed to the high density of hydrogen s-states present at the Fermi level. Furthermore, a metastable $Pm\bar{3}$ phase of clathrate $NaPH_6$ hydride are uncovered under 350 GPa, which displays an exceptional T_c of 201.4 K. These results suggest that ternary alkali metal Na-based hydrides hold promise as high-T_c superconductors under high pressure and offer critical insights into the design and synthesis of novel category high temperature superconductors.

I. INTRODUCTION

The strong electron-phonon coupling (EPC) and high-frequency phonon vibrations make metallic hydrogen a promising high-temperature superconductor [1–3]. However, the metallization pressure required for dense hydrogen exceeds 450 GPa [4, 5], which is still a challenge for current hydrostatic pressure experiments. A flexible strategy, "pre-compression" of hydrogen in hydrogen dominant hydrides proposed by Ashcroft [6] in 2004, can produce the metallic hydrogen at relatively low pressure conditions. Several high-temperature superconductors in hydrides at high pressure are discovered by this powerful strategy, such as, conventional sulfur hydrides (H_3S) [7, 8], lanthanum hydrides (LaH_{10}) [9, 10] and calcium hydrides (CaH_6), which are theoretically predicated to be metallic and subsequently confirmed by high-pressure experiments. These high-T_c superconductors exhibit high T_c values of 203 K at 150 GPa [11] and 250 K at 170 GPa [12, 13], and 215 K at 172 GPa [14], respectively. Therefore, the compressed hydrides are metallization at much lower pressures compared with the metallic hydrogen.

Since then, a serial of surprising metallic hydrides with rather high-T_c are searched by extensive theoretical predictions [15–22]. Sodalite-like clathrate MgH_6 is predicated with T_c higher than 200 K [21, 22] under high pressure [14, 15]. Semenok *et al.* have reported the detailed structure, electronic properties, and maximum T_c values for alkali metal and transition metal-based binary hydrides in a recent review [19], which offer active guidance for future synthesis of binary hydrides. As for rare-earth (RE) hydrides, Peng *et al.* have conducted symmetrical study for entire lanthanide series of elements, and the T_c values of energetically stable YH_{10} and LaH_{10} hydrides are 303 K and 288 K at high pressure [10]. We have also explored high T_c superconductivity in H-rich RE hydrides and identified the "second island" of high T_c superconductors in late Yb/Lu polyhydrides [23]. Moreover, the yttrium hydrides with high symmetrized H-cages in corresponding crystal structures are also potential superconductors. Some stable and metastable yttrium hydrides, such as YH_3, YH_6 and YH_9, are successfully predicated and confirmed by the later experiments [24–27].

Recent reports [28, 29] have identified ternary hydrides that undergo metallization at moderate pressures while exhibiting high T_c values, potentially even at room-temperature. Sun *et al.* have discovered the metastable Li_2MgH_{16} [30] ternary hydride with remarkably high T_c value of $\sim$ 473 K at 250 GPa. The doped Li atoms in Li_2MgH_{16} provide extra electrons to dissociate the H_2 molecules, which greatly improve the strong EPC and cause the high T_c superconductivity. Alkali metals (Li) and alkaline earth metals (Mg, Ca) can donate electrons [31–36] to enhance the T_c of hydrides. For example, phosphorus hydrides are metastable phases corresponding to elemental phosphorus and hydrogen [35–37]. The free-electron metal Li ([He] $2s^1$) doped metastable P-H binary hydrides, such as LiP_2H_{14} (169 K at 230 GPa) [38] and $LiPH_6$ (167 K at 200 GPa) [39], can produce stable high-T_c superconductors. By contrast, the atomic radius of sodium is about 1.8 Å, which is larger than that of lithium. The metallized pressures of sodium-based hydrides are, in principle, lower than those of lithium hydrides [40, 41]. For instance, Na_3FeH_7 and Na_3CoH_6 hydrides exhibit low synthesis pressures of about 10 GPa [42], and Na_2SiH_6 hydrides are known to form several hypervalent compounds which exhibit superionicity at rel-

atively low pressure.

In this work, we have conducted a systematic study on sodium metal doped in phosphorus hydrides, producing stabilized $NaPH_n$ ($n = 3$ - 8) ternary hydrides under high pressure. Energetic, structural, and electronic properties of the stable H-rich $NaPH_6$ and $NaPH_8$ hydrides indicate that $NaPH_6$ are energetic and dynamic stability at 200 GPa. Furthermore, the hexagonal layered $P\bar{6}m2$ phase of $NaPH_6$ is excellent superconductor with high $T_c \sim$ 112.2 K at 200 GPa, while cubic clathrate $Pm\bar{3}$ phase of $NaPH_6$ exhibits a T_c value of 201.4 K under 350 GPa. The Pm phase of $NaPH_8$ is metallic at 200 GPa with T_c of 55.9 K, suggesting that H-rich $NaPH_6$ and $NaPH_8$ hydrides are high T_c superconductors.

II. COMPUTATIONAL DETAILS

The candidate structures of ternary Na-P-H hydrides are predicted by CALYPSO code [43–45]. We perform the variable-composition crystal structure searches for $NaPH_n$ ($n = 3$ - 8) ranging from 1 f.u/cell to 4 f.u/cell at 100, 200, 300, 400 GPa. Total energy and electronic properties are calculated by using Vienna Ab initio Simulation Package (VASP) [46] with in Perdew-Burke-Ernzerhof [47] of exchange-correlation functional. The PAW potentials with the valence electrons $3s^1$ for Na, $3s^2 3p^3$ for P and $1s^1$ for H are adopted [48]. The valid PAW pseudopotentials have been verified by various works under high-pressure [10, 23, 49]. For Na-P-H hydrides, the detailed core radii from the pseudopotentials and the interatomic distances (in Supplemental Material [50]) indicate that the PAW pseudopotential could cause the solid and valid results under high-pressure calculations. To ensure the convergence of force and energy, we set the corresponding plane wave cutoff energy of 800 eV and Brillouin zone samplings of 0.20 $Å^{-1}$. The dynamical stability for predicated ternary Na-P-H hydrides are calculated by PHONOPY code [51] by using density functional perturbation theory (DFPT). The EPC and superconducting critical temperature (T_c) are calculated by QUANTUM-ESPRESSO package [52]. Ultrasoft pseudopotentials for Na, P, and H atoms are chosen with kinetic energy cutoff of 80 Ry. To get the EPC parameter λ, the Brillouin zone are sampled by much dense 24×24×24 for k-points and 6×6×6 q-point mesh (convergence tests are shown in Fig. S1. The T_c are estimated by Allen-Dynes modified McMillan equation [53],

$$T_c = \frac{\omega_{log}}{1.2} exp(\frac{-1.04(1+\lambda)}{\lambda - \mu^*(1+0.62\lambda)}) \quad (1)$$

which considers the strong-coupling and shape correction multipliers of f_1 and f_2.

$$f_1 = [1 + (\frac{\lambda}{2.46(1+3.8\mu^*)})^{\frac{3}{2}}]^{\frac{1}{3}} \quad (2)$$

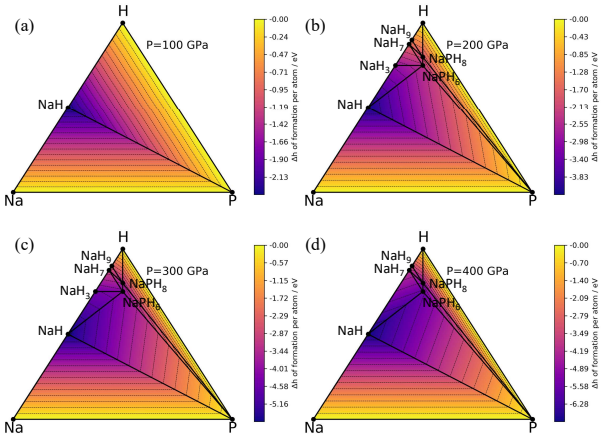

FIG. 1: (a-d) The 3D convex hulls constructed based on the formation enthalpies relate to the elemental Na, P and H at 100, 200, 300 and 400 GPa, the solid doted ($NaPH_6$ and $NaPH_8$) represent the energetically stable.

$$f_2 = 1 + \frac{(\frac{\bar{\omega}}{\omega_{log}} - 1)\lambda^2}{\lambda^2 + [1.82(1+6.3\mu^*)\frac{\bar{\omega}}{\omega_{log}}]^2} \quad (3)$$

$$T_c = f_1 f_2 \frac{\omega_{log}}{1.2} exp(\frac{-1.04(1+\lambda)}{\lambda - \mu^*(1+0.62\lambda)}). \quad (4)$$

The Coulomb pseudopotentials of $\mu^* = 0.10$ and 0.13 are taken in our calculation. The EPC constants of λ and ω_{log} are calculated as

$$\lambda = 2\int_0^\infty \frac{\alpha^2 F(\omega)}{\omega} d\omega \quad (5)$$

$$\omega_{log} = \exp[\frac{\lambda}{2}\int_0^\infty \frac{d\omega}{\omega}\alpha^2 F(\omega)\ln(\omega)]. \quad (6)$$

III. RESULTS AND DISCUSSION

We have explored the energetically stable structures of $NaPH_n$ ($n = 3$ - 8) hydrides at pressures ranging from 100-400 GPa. Clearly, the ternary stoichiometries of $NaPH_6$ and $NaPH_8$ hydrides are occurred in the three-dimension (3D) convex hulls, as depicted in Figure 1. Based on the formation enthalpies relative to the elemental Na, P, and H atoms, we have identified energetically stable binary NaH, NaH_3, NaH_7 and NaH_9 hydrides, and ternary $NaPH_6$ and $NaPH_8$ hydrides. Figure 1(a-d) shows that the ternary $NaPH_6$ and $NaPH_8$ hydrides remain stable up to 200 GPa. Additionally, in Figure S2(a, b, c) in the SM[50], we have presented the 3D convex hulls of $NaPH_6$ and $NaPH_8$ hydrides with respect to the stabilized binary NaH hydride and elemental P, H

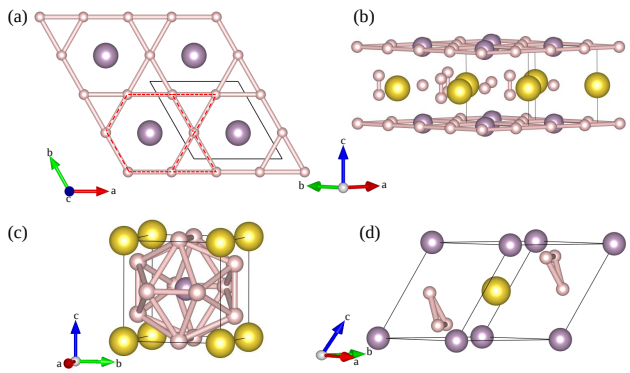

FIG. 2: Crystal structures for $NaPH_6$ (a-b) supercell of $P\bar{6}m2$ $NaPH_6$ at 200 GPa with different view, the Kagome lattice formed by H atoms in H-P layer, (c) $Pm\bar{3}$ structure at 350 GPa and (d) $R\bar{3}m$ structure at 200 GPa. The Sodium atoms are yellow, the Phosphorus atoms are purple and Hydrogen atoms are pink.

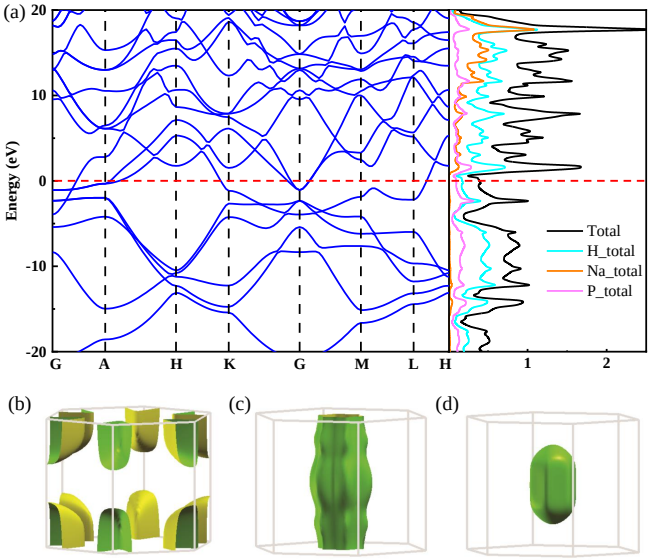

FIG. 3: (a) Calculated electronic band structures and density of states of $P\bar{6}m2$ $NaPH_6$, (b-d) the Fermi surface sheets of $P\bar{6}m2$ $NaPH_6$ structure at 350 GPa.

atoms. The enthalpy difference curves of $NaPH_6$ with respect to the $R\bar{3}m$ phase as functions of pressures are shown in Figure S3(a), which suggest that the hexagonal layered $P\bar{6}m2$ phase of $NaPH_6$ remains stable over the pressure range of 200 to 400 GPa. Our structure predictions have also uncovered two metastable $R\bar{3}m$ and $Pm\bar{3}$ phases of $NaPH_6$. The monoclinic Pm phase of $NaPH_8$ is identified as the ground state structure at high pressure from 200 to 350 GPa, as illustrated in Figure S3(b). Figure S4-6 displays the phonon dispersion curves of the $P\bar{6}m2$, $R\bar{3}m$, and $Pm\bar{3}$ phases of $NaPH_6$, indicating that the $P\bar{6}m2$ phase is thermodynamically stable within the pressure range of 150 to 400 GPa.

The detailed crystal structures of $NaPH_6$ hydrides under selected pressures are displayed in Figure 2 and Figure S7. The corresponding structure parameters are summarized in Table S1. Typically, H-rich clathrate structures are observed in binary and ternary H-rich superconductors. However, the most stable structure of $NaPH_6$ hydride at 200 GPa is a layered $P\bar{6}m2$ phase, as depicted in Figure 2(a,b), which consists of H-P and Na-H layers. The H_2 units are bonded with the P-H and Na-H layers, the corresponding H-H distance is about 0.774 Å. The H atoms in P-H layers form a Kagome lattice (in Figure 2(a)), while the P atoms are centered within each Kagome framework [54]. Additionally, a H-rich clathrate structure of $NaPH_6$ hydride with $Pm\bar{3}$ symmetry is identified. The cubic $Pm\bar{3}$ phase of $NaPH_6$ hydride is metallic and stable at 350 GPa, as depicted in Figure 2(c). The H_{12} cages are surrounded by P atoms, which is similar to the previously reported $LiPH_6$ hydride [39]. Another metastable phase of $NaPH_6$ is observed in the structural searches at 200 GPa, which is a trigonal $R\bar{3}m$ structure, as shown in Figure 2(d), where the H atoms are arranged in triangular H_3 units. Na atoms are located at the eight corners of the lattice, while the P atoms are situated in the body-centered lattice. Although the trigonal $R\bar{3}m$ phase and cubic $Pm\bar{3}$ phase of $NaPH_6$ possess formation enthalpies that are approximately 0.044 eV/atom and 0.182 eV/atom higher, respectively, than that of the ground state $P\bar{6}m2$ phase at 200 GPa, they are still regarded as metastable phases due to their mechanical and thermodynamic instability.

In Figure 3(a), we present the electronic band structure and density of states (DOS) for the most stable $P\bar{6}m2$ phase of $NaPH_6$ at 200 GPa. The flat electronic bands crossing the Fermi level indicate the metallic character of the $P\bar{6}m2$ phase. The H-s states contribute to half of the total DOS at the Fermi level, and their high values suggest that the $P\bar{6}m2$ phase of $NaPH_6$ is a potential high-T_c superconductor [23]. The Fermi surface of the $P\bar{6}m2$ phase, shown in Figure 3(b-d), reveals that the electron packages are located around the Γ point. Furthermore, we display the detailed DOS and Fermi surface sheets for the metastable $R\bar{3}m$ and $Pm\bar{3}$ phases at 350 GPa in Figure S10, which show that both $R\bar{3}m$ and $Pm\bar{3}$ phases of $NaPH_6$ are metallic with relatively large number of H-s states at the Fermi level.

Motivated by the metallic properties of $NaPH_6$ hydride, we have calculated the EPC parameters for both stable and metastable hydrides at high pressure. The electronic density of states at Fermi level (N_{Ef}), detailed EPC parameter λ, the logarithmic average phonon frequency ω_{log}, and the superconductivity T_c are summarized in Table 1. The results indicate that layered $P\bar{6}m2$ structure possess a high-T_c of 112.2 K (λ = 1.313) at 200 GPa and 93.4 K (λ = 0.904) at 350 GPa when μ^* =

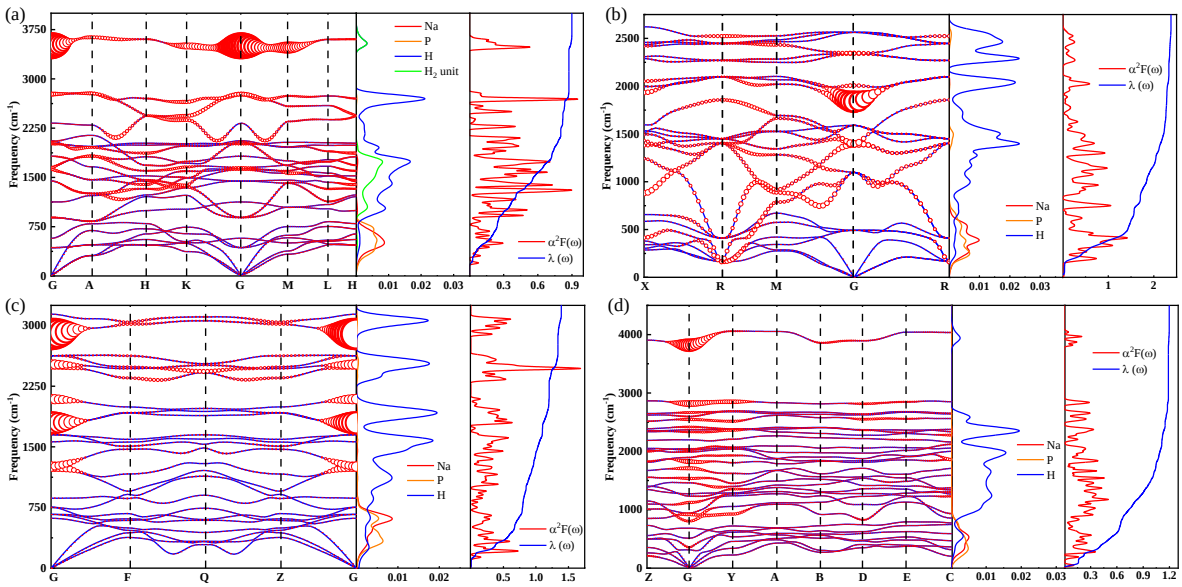

FIG. 4: Phonon dispersion curves (the radius of red circle is parallel to phonon linewidths), phonon density of states (PHDOS) projected on Na, P and H atoms, and Eliashberg spectral function $\alpha^2F(\omega)$ together with the electron-phonon integral $\lambda(\omega)$ at 350 GPa for (a) $P\bar{6}m2$ phase of $NaPH_6$, (b) $Pm\bar{3}$ phase of $NaPH_6$, (c) $R\bar{3}m$ phase of $NaPH_6$ and (d) Pm phase of $NaPH_8$.

TABLE I: Predicted superconducting properties of Ternary Na-P-H high-temperature superconductivity polyhydrides at different pressure, T_c are estimated by McMillan equation and with the Allen–Dynes modified McMillan equation .

Hydrides	Space group	Pressure (GPa)	N_{Ef} (States/Ry/f.u.)	λ	ω_{log}, K	T_c (K)		$f_1f_2T_c$ (K)
						$\mu^* = 0.10$	$\mu^* = 0.13$	$\mu^* = 0.10$
$NaPH_6$	187 ($P\bar{6}m2$)	150	4.231	3.311	377.277	70.7	67.5	110.5
	187 ($P\bar{6}m2$)	200	3.766	1.313	1128.264	112.2	100.8	
	187 ($P\bar{6}m2$)	300	3.677	0.984	1417.528	96.3	82.4	
	187 ($P\bar{6}m2$)	350	3.601	0.904	1581.039	93.4	78.2	
	187 ($P\bar{6}m2$)	400	3.596	0.883	1503.430	85.1	70.8	
	166 ($R\bar{3}m$)	200	2.652	1.289	854.109	83.2	74.6	
	166 ($R\bar{3}m$)	300	3.173	1.496	905.954	103.0	93.9	118.8
	166 ($R\bar{3}m$)	350	2.633	1.313	964.058	95.9	86.1	
	200 ($Pm\bar{3}$)	340	5.375	2.257	997.160	155.0	145.6	196.1
	200 ($Pm\bar{3}$)	350	5.393	2.347	1009.917	160.6	151.2	201.4
	200 ($Pm\bar{3}$)	400	5.065	2.235	726.923	112.3	105.5	145.2
$NaPH_8$	6 (Pm)	200	2.748	1.467	500.387	55.9	50.8	
	6 (Pm)	300	1.701	0.670	1995.376	62.1	46.6	
	6 (Pm)	350	2.456	1.192	764.332	67.8	60.1	

0.10. The layered $P\bar{6}m2$ phase represents a novel category of high T_c hydrides, which has expanded the range of known covalent and clathrate superhydrides [29]. Our calculations indicate that the EPC λ value for the $Pm\bar{3}$ phase of $NaPH_6$ is approximately 2.347. For EPC $\lambda >$ 1.5, by considering the Allen-Dynes modified McMillan equation, the T_c superconductivity of cubic $Pm\bar{3}$ phase of $NaPH_6$ is determined to be 201.4 K, which is higher than the T_c of approximately 167.3 K for the similar cubic $Pm\bar{3}$ phase of $LiPH_6$ [39]. Furthermore, the metastable trigonal $R\bar{3}m$ phase of $NaPH_6$ exhibits a T_c value of 95.9 K ($\lambda = 1.313$) at 350 GPa. The remarkable superconductivity observed in $NaPH_6$ suggests that Na atoms could provide electrons to increase the contribution of DOS of atomic hydrogen around the Fermi level, and result in high T_c values. Based on the N_{Ef} values presented in Table 1, it can be observed that high N_{Ef} values correspond to high T_c values, as evidenced by the $P\bar{6}m2$, $R\bar{3}m$,

and $Pm\bar{3}$ phases of $NaPH_6$ exhibiting higher T_c values at selected pressures. For example, the $P\bar{6}m2$ phase displays a T_c of 112.2 K (with a N_{Ef} value of $\sim$ 3.766), while the $Pm\bar{3}$ phase exhibits a T_c of 201.4 K (with a N_{Ef} value of $\sim$ 5.393). Comparing the superconductivity trends with the cubic $Pm\bar{3}$ phase of $LiPH_6$, it can be inferred that the alkali metal Na can stabilize P-H hydrides at high pressure and enhance the EPC, leading to highly T_c superconductivity.

To further explore the superconductivity mechanism in diverse structures of $NaPH_6$ hydrides, we have calculated the phonon dispersion curves, phonon density of states (PHDOS) projected on Na, P and H atoms, and Eliashberg spectral function $\alpha^2F(\omega)$ together with the electron-phonon integral $\lambda(\omega)$ at 350 GPa, as displayed in Figure 4. The phonon modes for layered $P\bar{6}m2$ phase (Figure 4(a)) exhibit two distinct frequency ranges: Na and P atoms contribute minimally to the overall EPC λ due to their substantial atomic masses in the low-frequency range (0-750 cm^{-1}). Meantime, the high-frequency region (>750 cm^{-1}) is predominantly associated with atomic H atom vibrations and H_2 molecules, contributing significantly to the total EPC λ (up to 67 %), similar to H-dominated binary high-T_c superconductors such as H_3S [7, 11] and lanthanide hydrides [10, 12, 13]. In Figure 4(b), the clathrate $Pm\bar{3}$ phase of $NaPH_6$ exhibits a compelling soft phonon mode in the middle frequency (250 -1500 cm^{-1}) at R point. The radius of the red circle on the phonon dispersion curve represents the strength of EPC λ, indicating that the considerable phonon linewidths mainly originate from the H-H vibration soft phonon modes around R and Γ point for $Pm\bar{3}$ $NaPH_6$ at 350 GPa. The phonon modes in the low frequency region (< 750 cm^{-1}) predominantly related to the Na/P atoms and a portion of H-H soft phonon, resulting to 70 % of total EPC λ, while the atomic H-H vibration phonon modes dominate the high frequency > 750 cm^{-1} with 30 % of EPC λ (in Figure 4(b)). Interestingly, the vibrational range of hydrogen atoms in trigonal $R\bar{3}m$ phase of $NaPH_6$ is different from layered and cubic structures, which appear in the entire vibration frequency regions (in Figure 4 (c)). For $R\bar{3}m$ phase of $NaPH_6$ hydride, H atoms combined with Na and P atoms contribute about 45 % of the total EPC λ in the low frequency range. The hydrogen plays the dominating role in strong EPC, leading to high-T_c ternary atomic hydrides superconductors. Overall, among the three phases of $NaPH_6$ hydride superconductors, metastable $Pm\bar{3}$ phase with atomic hydrogen possesses the highest T_c value of approximately 201.4 K at 350 GPa, attributed to the Na/P vibrations in the low-frequency region contributing 70 % of the total EPC λ. Meanwhile, the layered $P\bar{6}m2$ ground state and trigonal $R\bar{3}m$ metastable for $NaPH_6$ display T_c values of around 93.4 K and 95.9 K at 350 GPa, respectively.

We next calculate the projected crystal orbital Hamiltonian population (pCOHP)[55–57] to evaluate the chemical bonding in Na-P-H hydrides, which can provide critical insights into the relationships between superconductivity and structure among the different phases of $NaPH_6$. Figure 5(a) reveals strong H-H bonding in layered $P\bar{6}m2$ phase of $NaPH_6$, evidenced by the prominent features of occupied antibonding states near the Fermi level. The substantial antibonding states of H-H bonding, including the H-H bonding in H_2 molecular accord with the dominant contribution of 67 % to the total EPC λ in $P\bar{6}m2$ phase of $NaPH_6$ at 350 GPa. It is noteworthy that the Na-H and P-H bonding states are qualitatively similar in cubic $Pm\bar{3}$ and trigonal $R\bar{3}m$ phases of $NaPH_6$ (Figure 5 (b-c)), with occupied bonding states below and antibonding states above the Fermi level, respectively. Moreover, in the cubic $Pm\bar{3}$ phase of $NaPH_6$, the H atoms contribute to strong H-H bonding states near the Fermi level (Figure 5 (c)), indicating the highest T_c values. Table S1 presents the detailed Bader charges of Na, P and H atoms of $NaPH_6$ hydrides at 350 GPa, suggesting the number of electrons transferred from Na/P to

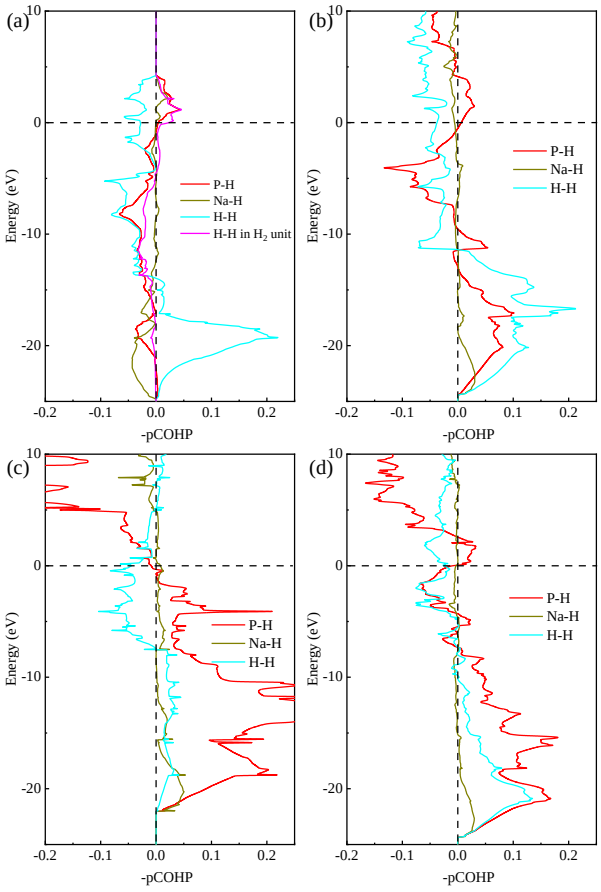

FIG. 5: Projected crystal orbital Hamiltonian Population (-pCOHP) of the predicted compounds (a) $P\bar{6}m2$ phase of $NaPH_6$, (b) $R\bar{3}m$ phase of $NaPH_6$, (c) $Pm\bar{3}$ phase of $NaPH_6$ and (d) Pm phase of $NaPH_8$ at 350 GPa.

H atoms. For the three phases of $NaPH_6$ hydrides, the partial charges transferred in the layered $P\bar{6}m2$ phase are -0.61e and -0.62e for Na and P, respectively. Similar values are observed in cubic $Pm\bar{3}$ (-0.47e for Na and -1.29e for P) and trigonal $R\bar{3}m$ (-0.57e for Na and -2.53e for P) phases of $NaPH_6$ at 350 GPa, with H atoms accepting all electrons from the Na and P atoms. The formation of metallic H-H bonds by charge transfer from Na and P atoms, induces the high frequency vibration and causes the high-T_c superconductivity of $NaPH_6$. For ground state layered $P\bar{6}m2$ phase of $NaPH_6$, the 2h and 2c sites of H atoms represent the H_2 molecules, corresponding to nearly negligible electron transfer of 0.03e, respectively. The significant degree of electron transfer from Na/P atoms to H atoms in the ternary $P\bar{6}m2$, $R\bar{3}m$ and $Pm\bar{3}$ hydrides promotes the formation of Na-H and P-H bonds, as well as high-frequency hydrogen vibrations, which is consistent with the above EPC calculations.

In fact, we have found another stable stoichiometry of $NaPH_8$ in ternary Na-P-H hydrides at 200 GPa. It is also a layered structure with Pm symmetry, as shown in Figure S7(c), which is composed of Na-H_2-H and P-H layers. The H-H distance within the H_2 unit is approximately 0.742 Å. As shown in Figure S9(b), the calculated band structures and DOS indicate the Pm phase of $NaPH_8$ possesses a limited metallic character. The corresponding EPC calculations reveal that the Pm phase of $NaPH_8$ shows a T_c value of 67.8 K ($\lambda \sim 1.192$), which is lower than the layered $P\bar{6}m2$ phase of $NaPH_6$ ($T_c \sim 93.4$ K) at 350 GPa. For the Pm phase of $NaPH_8$, the analogous vibration phonon modes are also presented in Figure 4 (d). The soft phonon modes around Γ point indicate the H atom vibrations effectively enhance the EPC, and H atoms dominate the high-frequency regions (>750 cm^{-1}) with 42 % of the total λ.

V. CONCLUSIONS

In summary, we have explored the crystal structures and superconductivity of H-rich Na-P-H ternary hydrides at 100 - 400 GPa, by using structure prediction methods and first-principles calculations. We have discovered two stable stoichiometries of $NaPH_6$ and $NaPH_8$ in ternary Na-P-H hydrides under 200 GPa. The $P\bar{6}m2$ phase of $NaPH_6$ has been verified as the novel ternary layered H-rich superconductor with a high T_c value of 112.2 K under 200 GPa. Interestingly, the metastable clathrate $Pm\bar{3}$ phase of $NaPH_6$ is identified with a substantial T_c value of 201.4 K at 350 GPa. Our calculations demonstrate that the high T_c of $NaPH_6$ under high pressure is due to the high density of H-s states at the Fermi level, and H atoms contribute to strong EPC interactions in ternary sodium phosphorus hydrides. These findings enrich the understanding of alkali metal phosphorus hydrides under high pressure and provide vital perspectives for further exploration of innovative classes of high temperature superconductors.

ACKNOWLEDGEMENTS

This work was supported by the National Natural Science Foundation of China (Nos. 12111530103, and 12174352). W.G Sun acknowledge funding from the Key Research Project in University of Henan Province under Grant No. 22A140025, and Natural Science Foundation of Henan Province No. 232300420352.

* Electronic address: fpeng@calypso.cn
† Electronic address: lucheng@calypso.cn

[1] P. Loubeyre, F. Occelli, and P. Dumas, Nature **577**, 631 (2020).
[2] P. Loubeyre, F. Occelli, and R. LeToullec, Nature **416**, 613 (2002).
[3] N. W. Ashcroft, Phys. Rev. Lett. **21**, 1748 (1968).
[4] J. M. McMahon and D. M. Ceperley, Phys. Rev. B **84**, 144515 (2011).
[5] P. Cudazzo, G. Profeta, A. Sanna, A. Floris, A. Continenza, S. Massidda, and E. K. U. Gross, Phys. Rev. Lett. **100**, 257001 (2008).
[6] N. W. Ashcroft, Phys. Rev. Lett. **92**, 187002 (2004).
[7] D. Duan et al., Sci. Rep. **4**, 6968 (2014).
[8] Y. Li, J. Hao, H. Liu, Y. Li, and Y. Ma, J. Chem. Phys. **140**, 174712 (2014).
[9] H. Liu, I. I. Naumov, R. Hoffmann, N. W. Ashcroft, and R. J. Hemley, Proc. Natl. Acad. Sci. U. S. A. **114**, 6990 (2017).
[10] F. Peng, Y. Sun, C. J. Pickard, R. J. Needs, Q. Wu, and Y. Ma, Phys. Rev. Lett. **119**, 107001 (2017).
[11] A. P. Drozdov, M. I. Eremets, I. A. Troyan, V. Ksenofontov, and S. I. Shylin, Nature **525**, 73 (2015).
[12] A. P. Drozdov, P. P. Kong, V. S. Minkov, S. P. Besedin, M. A. Kuzovnikov, S. Mozaffari, L. Balicas, F. F. Balakirev, D. E. Graf, V.B. Prakapenka *et al.*, Nature **569**, 528 (2019).
[13] M. Somayazulu, M. Ahart, A. K. Mishra, Z. M. Geballe, M. Baldini, Y. Meng, V. V. Struzhkin, and R. J. Hemley, Phys. Rev. Lett. **122**, 027001 (2019).
[14] L. Ma, K. Wang, Y. Xie, X. Yang, Y. Wang, M. Zhou, H. Liu, X. Yu, Y. Zhao, H. Wang, G. Liu, Y. Ma, Phys. Rev. Lett. **128**, 167001 (2022).
[15] Z. Li, X. He, C. Zhang, X. Wang, S. Zhang, Y. Jia, S. Feng, K. Lu, J. Zhao, J. Zhang *et al.* Nat. Commun. **13**, 2863 (2022).
[16] D. F. Duan, Y. X. Liu, Y. B. Ma, Z. Shao, B. B. Liu, and T. Cui, Natl. Sci. Rev. **4**, 121 (2017).
[17] E. Zurek and T. G. Bi, J. Chem. Phys. **150**, 050901 (2019).
[18] J. A. Flores-Livas, L. Boeri, A. Sanna, G. Profeta, R. Arita, and M. Eremets, Phys. Rep. **856**, 1 (2020).
[19] D. V. Semenok, I. A. Kruglov, I. A. Savkin, A. G. Kvashnin, and A. R. Oganov, Curr. Opin. Solid State Mater. Sci. **24**, 100808 (2020).

[20] D. C. Lonie, J. Hooper, B. Altintas, and E. Zurek, Phys. Rev. B **87**, 054107 (2013).

[21] H. Wang, J. S. Tse, K. Tanaka, T. Iitaka, and Y. Ma, Proc. Natl. Acad. Sci. U. S. A. **109**, 6463 (2012).

[22] X. Feng, J. Zhang, G. Gao, H. Liu, and H. Wang, RSC Adv. **5**, 59292 (2015).

[23] W. Sun, X. Kuang, H. D. J. Keen, C. Lu, and A. Hermann, Phys. Rev. B **102**, 144524 (2020).

[24] I. A. Troyan, D. V. Semenok, A. G. Kvashnin, A. V. Sadakov, O. A. Sobolevskiy, V. M. Pudalov, A. G. Ivanova, V. B. Prakapenka, E. Greenberg, A. G. Gavriliuk *et al.*, Adv. Mater. **33**, e2006832 (2021).

[25] J. Purans, A.P. Menushenkov, S.P. Besedin, A.A. Ivanov, V.S. Minkov, I. Pudza, A. Kuzmin, K.V. Klementiev, S. Pascarelli, O. Mathon *et al.*, Nat. Commun. **12**, 1765 (2021).

[26] E. Snider, N. Dasenbrock-Gammon, R. McBride, X. Wang, N. Meyers, K. V. Lawler, E. Zurek, A. Salamat, and R. P. Dias, Phys. Rev. Lett. **126**, 117003 (2021).

[27] Y. Li, J. Hao, H. Liu, J. S. Tse, Y. Wang, and Y. Ma, Sci. Rep. **5**, 9948 (2015).

[28] X. Zhang, Y. Zhao, and G. Yang, Wiley Interdiscip. Rev. Comput. Mol. Sci. **12**, e1582 (2021).

[29] M. Du, W. Zhao, T. Cui, and D. Duan, J. Phys. Condens. Matter **34**, 173001 (2022).

[30] Y. Sun, J. Lv, Y. Xie, H. Liu, and Y. Ma, Phys. Rev. Lett. **123**, 097001 (2019).

[31] X. Liang, A. Bergara, L. Wang, B. Wen, Z. Zhao, X.-F. Zhou, J. He, G. Gao, and Y. Tian, Phys. Rev. B **99**, 100505 (2019).

[32] H. Xie, D. Duan, Z. Shao, H. Song, Y. Wang, X. Xiao, D. Li, F. Tian, B. Liu, T. Cui, J. Phys. Condens. Matter **31**, 245404 (2019).

[33] Y. Yan, T. Bi, N. Geng, X. Wang, and E. Zurek, J. Phys. Chem. Lett. **11**, 9629 (2020).

[34] D. Meng, M. Sakata, K. Shimizu, Y. Iijima, H. Saitoh, T. Sato, S. Takagi, and S. Orimo, Phys. Rev. B **99**, 024508 (2019).

[35] J. A. Flores-Livas, M. Amsler, C. Heil, A. Sanna, L. Boeri, G. Profetsa, C. Wolverton, S. Goedecker, and E. Gross, Phys. Rev. B **93**, 020508 (2016).

[36] A. Shamp, T. Terpstra, T. Bi, Z. Falls, P. Avery, and E. Zurek, J. Am. Chem. Soc. **138**, 1884 (2016).

[37] Y. Yuan, Y. Li, G. Fang, G. Liu, C. Pei, X. Li, H. Zheng, K. Yang, and L. Wang, Natl. Sci. Rev. **6**, 524 (2019).

[38] X. Li, Y. Xie, Y. Sun, P. Huang, H. Liu, C. Chen, and Y. Ma, J. Phys. Chem. Lett. **11**, 935 (2020).

[39] Z. Shao, D. Duan, Y. Ma, H. Yu, H. Song, H. Xie, D. Li, F. Tian, B. Liu, T. Cui, Npj Comput. Mater. **5**, 104 (2019).

[40] C. Pépin, P. Loubeyre, F. Occelli, and P. Dumas, Proc. Natl. Acad. Sci. U.S.A. **112**, 7673 (2015).

[41] Y. M. Chen, H. Y. Geng, X. Z. Yan, Y. Sun, Q. Wu, and X. R. Chen, Inorg. Chem. **56**, 3867 (2017).

[42] K. Spektor, W. A. Crichton, S. Filippov, S. I. Simak, A. Fischer, and U. Häussermann, Inorg. Chem. **59**, 16467 (2020).

[43] J. Lv, Y. Wang, L. Zhu, and Y. Ma, J. Chem. Phys. **137**, 084104 (2012).

[44] Y. Wang, J. Lv, L. Zhu, and Y. Ma, Phys. Rev. B **82**, 094116 (2010).

[45] B. Gao, P. Gao, S. Lu, J. Lv, Y. Wang, and Y. Ma, Sci. Bull. **64**, 301 (2019).

[46] G. Kresse and J. Furthmüller, Comput. Mater. Sci. **6**, 15 (1996).

[47] J. P. Perdew, K. Burke, and M. Ernzerhof, Phys. Rev. Lett. **77**, 3865 (1996).

[48] G. Kresse and D. Joubert, Phys. Rev. B **59**, 1758 (1999).

[49] A. R. Oganov, J. Chen, C. Gatti, Y. Ma, Y. Ma, C. W. Glass, Z. Liu, T. Yu, O.O. Kurakevych, V. L. Solozhenko, Nature, **457** 863-867 (2009).

[50] See Supplemental Material at http://link.aps.org/xxx for the 3D convex hulls, phonon dispersion curves, crystal structures, density of states, Bader charges and crystallographic lattice information.

[51] A. Togo and I. Tanaka, Scr. Mater. **108**, 1 (2015).

[52] P. Giannozzi, S. Baroni, N. Bonini, M. Calandra, R. Car, C. Cavazzoni, D. Ceresoli, G.L. Chiarotti, M. Cococcioni, I. Dabo *et al.*, J. Phys. Condens. Matter **21**, 395502 (2009).

[53] P. B. Allen and R. C. Dynes, Phys. Rev. B **12**, 905 (1975).

[54] Q. Chen, S. C. Bae, and S. Granick, Nature **469**, 381 (2011).

[55] R. Dronskowski and P. E. Bloechl, J. Phys. Chem. **97**, 8617 (1993).

[56] V. L. Deringer, A. L. Tchougreeff, and R. Dronskowski, J. Phys. Chem. A **115**, 5461 (2011).

[57] S. Maintz, V. L. Deringer, A. L. Tchougreeff, and R. Dronskowski, J. Comput. Chem. **37**, 1030 (2016).